Role of Water on Unfolding Kinetics of Helical Peptides Studied by Molecular Dynamics Simulations

P. Doruker and I. Bahar
Polymer Research Center, Chemical Engineering Department, Bogazici University, and TUBITAK Advanced Polymeric Materials Research Center, Bebek 80815, Istanbul, Turkey

ABSTRACT Molecular dynamics simulations have been carried out with four polypeptides, Ala_{13}, Val_{13}, Ser_{13}, and $Ala_4Gly_5Ala_4$, in vacuo and with explicit hydration. The unfolding of the polypeptides, which are initially fully α-helix in conformation, has been monitored during trajectories of 0.3 ns at 350 K. A rank of Ala < Val < Ser < Gly is found in the order of increasing rate of unwinding. The unfolding of Ala_{13} and Val_{13} is completed in hundreds of picoseconds, while that of Ser_{13} is about one order of magnitude faster. The helix content of the peptide containing glycine residues falls to zero within a few picoseconds. Ramachandran plots indicate quite distinct equilibrium distributions and time evolution of dihedral angles in water and in vacuum for each residue type. The unfolding of polyalanine and polyvaline helices is accelerated due to solvation. In contrast, polyserine is more stable in water compared to vacuum, because its side chains can form intramolecular hydrogen bonds with the backbone more readily in vacuum, which disrupts the helix. Distribution functions of the spatial and angular position of water molecules in the proximity of the polypeptide backbone polar groups reveal the stabilization of the coiled structures by hydration. The transition from helix to coil is characterized by the appearance of a new peak in the probability distribution at a specific location characteristic of hydrogen bond formation between water and backbone polar groups. No significant insertion of water molecules is observed at the precise onset of unwinding, while (i, i+3) hydrogen bond formation is frequently detected at the initiation of α-helix unwinding.

INTRODUCTION

It has long been accepted that individual protein fragments or short polypeptides should not form helices in water, following the Zimm-Bragg theory of helix-coil equilibrium (Zimm and Bragg, 1959). The C- and S-peptide fragments of ribonuclease A were the first examples with significant α-helix formation in water near 0°C (Brown and Klee, 1971; Bierzynski et al., 1982; Kim and Baldwin, 1984). Later other de novo designed peptides (Marqusee and Baldwin, 1987; Lyu et al., 1989; Bradley et al., 1990; Huyghues-Despointes et al., 1993) have been reported to assume helical structure at low temperature. The unusually stable α-helix formation observed in 16-residue alanine-based peptides has been attributed to the high helix-forming potential of alanines (Marqusee et al., 1989).

Helical propensity scales for amino acids have been obtained either directly from stability experiments in host-guest systems (Sueki et al., 1984; Lyu et al., 1990; O'Neil and DeGrado, 1990; Padmanabhan et al., 1990; Wojcik et al., 1990; Chakrabartty et al., 1994) including site-directed mutagenesis at specific sites (Horovitz et al., 1992; Blaber et al., 1993), or from the statistical analysis of known structures (Chou and Fasman, 1978). A recent review (Chakrabartty and Baldwin, 1995) summarizes experimental and theoretical work on the stability of α-helices. The resulting rankings exhibit some dependence on the detection method, as well as on the sequence context (Padmanabhan et al., 1990). The extent to which the helical propensities reflect the intrinsic properties of individual residues irrespective of the environment or result from solvent effects is not yet resolved. Likewise, the relative contributions of intramolecular and intermolecular effects to α-helix winding/unwinding kinetics are not well-established.

Molecular dynamics (MD) simulations provide one direct approach for understanding the conformational preferences of amino acids and for gaining insights into the mechanism of helix formation, stabilization, and disruption, as reviewed by Brooks and Case (1993). Simulations of helix-coil transitions in peptides may be classified into two broad groups: 1) those investigating the thermodynamics of helix-coil transition, and 2) those examining the kinetics of the folding/unfolding. The former group of studies focuses primarily on the distributions of conformational states, or on the free energy changes associated with helix-coil transition (Andersen and Hermans, 1988; Tobias and Brooks, 1991; Tobias et al., 1991; Yun and Hermans, 1991; Hermans et al., 1992; Wang et al., 1995). These provide, for example, estimates of the Zimm-Bragg parameters as a function of amino acid type (Hermans et al., 1992; Wang et al., 1995). The second group of simulations, on the other hand, concentrates on the time evolution or on the mechanism of helix formation or disruption (Soman et al., 1991, 1993; DiCapua et al., 1990, 1991; Daggett et al., 1991; Daggett and Levitt, 1992). Activation energies for helix-to-coil transitions are extracted from these simulations by comparing the unfold-

Received for publication 31 July 1996 and in final form 25 February 1997.

Address reprint requests to I. Bahar, Polymer Research Center, School of Engineering, Bogazici University, Bebek 80815, Istanbul, Turkey. Tel.: 011-90-212-2631540, ext. 2003; Fax: 011-90-212-257-932; E-mail: bahar@indigo.bme.boun.edu.tr.

Dr. Doruker's present address is Maurice Morton Institute of Polymer Science, The University of Akron, Akron, OH 44325-3909.

0006-3495/97/06/2445/12 $2.00

ing rates at different temperatures (Daggett and Levitt, 1992).

A conclusive picture could not be reached so far on the mechanism of helix-coil transitions, presumably because of the difficulty of accurately sampling the high energy barrier region. For example, a tendency of (i, i+4) hydrogen bonds to switch to bifurcated $\alpha/3^{10}$-helical forms or to (i, i+3) hydrogen bonds has been identified as an important mechanism in helix unwinding (Soman et al., 1991, 1993), as well as the insertion of water molecules into helical hydrogen bonds (Soman et al., 1991; DiCapua et al., 1990, 1991). The latter is also suggested by an analysis of crystal structures (Sundaralingam and Sekharudu, 1989). According to the thermodynamic analysis of Tobias and Brooks (1991), on the other hand, water molecules do not form a three-centered hydrogen bond with the $(CO)_i$ and $(NH)_{i+4}$ groups of α-helices during the initiation of helix unwinding; instead, the $(CO)_i$ and $(NH)_{i+4}$ groups are solvated by different water molecules as the helix unwinds. Simulations of oligoalanines unfolding by Daggett and Levitt (1992) have not shown any evidence of helix destabilization upon water insertion.

In the present study, we examine the residue-specific unfolding of helical peptides, and the interference of water molecules as a function of the type of the amino acid. MD simulations are carried in vacuum and with explicit water molecules. We consider short helical polypeptides of alanine, valine, serine, and glycine. Radial and angular distributions of water molecules in the neighborhood of specific residues will be analyzed. The following issues will be considered: 1) are the dihedral angle distributions, conventionally determined from short-range intramolecular interactions (Brant et al., 1967), reproducible in MD simulations, uninfluenced by the solvation? 2) to what extent and in which direction do interactions with water affect the unfolding rates of particular amino acids in helical state? 3) is it possible to observe a direct correlation between the loci of water molecules and the conformational transitions of the backbone? Results regarding these issues will be presented and discussed in the Results section. We will also focus on the onset of unwinding to identify which mechanisms dominate the helix-to-coil transition. The latter will be shown to be highly residue-specific.

METHODS

MD simulations are carried out using the GROMOS87 simulation package (van Gunsteren and Berendsen, 1987). Four different model polypeptides, each comprising 13 residues, are simulated separately in vacuum and in the presence of explicit water molecules at 350 K and 1 bar, as summarized in Table 1. The primary structures of the polypeptides are Ala_{13}, Val_{13}, Ser_{13}, and $Ala_4Gly_5Ala_4$. The zwitterionic form of the peptide backbone is used, so the N- and C-termini are NH_3^+ and COO^-. The polypeptides are designated as pAla, pVal, pSer, and pGly for simplicity. Simulations in water and vacuum are differentiated by the suffix *w* and *v*, respectively. Two or more independent runs starting with different initial Gaussian velocities have been performed for each model chain in each medium so as to capture the reproducible features and diminish the statistical errors.

The initial conformations are taken to be right-handed α-helix. Bond lengths are constrained by the *Shake* algorithm (Ryckaert et al., 1977), which permits the adoption of 2-fs step sizes. The standard parameter set 37C4 of GROMOS87 is used for atomic interactions. The simple point charge (SPC) model (Berendsen et al., 1981) is adopted for water molecules. Non-bonded interactions are cut off at 0.8 nm, a value which has proven to provide an adequate description of the helix-coil equilibrium energetics in polypeptides (Wang et al., 1995). Use of a shorter cutoff distance would underestimate the stability of helices (Schreiber and Steinhauser, 1992). Steepest descent energy minimization of 50 steps, and 2-ps equilibration periods with strong coupling to an external heat and pressure bath (Berendsen et al., 1984) at 350 K and 1 bar, are performed before each MD run. Simulations of 0.3 ns are then performed in each case, except for pGly-*v*, which was extended to 1 ns. Temperature and pressure scaling parameters (Berendsen et al., 1984) of 0.1 ps and 0.5 ps, respectively, are adopted. The atomic coordinates are saved every 0.25 ps, resulting in 1200 snapshots of structures recorded in each independent run of 0.3 ns.

The box sizes and numbers of water molecules are chosen such that, after equilibration, a water layer of thickness $\geq$0.7 nm surrounds each solvent-exposed atom. Previous simulations of macromolecules in solution demonstrated that results are not significantly affected by the size of the simulation box, provided that the radius of gyration R_g of the chain is in the range $R_g/L < 0.25$, L being the edge of the cubic box (Bahar et al., 1993; Doruker and Bahar, 1993). Due to the asymmetry of the original conformations, rectangular boxes are adopted here. The x-, y-, and z-components of the instantaneous radii of gyration (R_{gx}, R_{gy}, and R_{gz}) were monitored in relation to the edges L_x, L_y, and L_z of the simulation box, to verify that the ratios R_{gi}/L_i (i = x, y, and z) remained within the acceptable range during simulations. Simulations performed with a larger size box for Ala_{13} (see Table 1) also confirmed that the further increase in the thickness of

TABLE 1 Model chains and environment in simulations

Polypeptide	Model	No. of waters	Simulation box sizes (Å)		
			x	y	z
Ala_{13}	pAla-*w*	540	21.391	22.786	36.110
Ala_{13}	pAla-*w*	711	24.391	25.786	36.110
Val_{13}	pVal-*w*	677	24.003	25.328	36.110
Ser_{13}	pSer-*w*	627	23.443	24.245	36.230
$Ala_4Gly_5Ala_4$	pGly-*w*	544	21.391	22.786	36.110
Ala_{13}	pAla-*v*	vacuum			
Val_{13}	pVal-*v*	vacuum			
Ser_{13}	pSer-*v*	vacuum			
$Ala_4Gly_5Ala_4$	pGly-*v*	vacuum			

At least two independent runs were performed for each of the tabulated systems. Simulations for pVal were repeated with different geometry and energy parameters for the side chain.

hydration shell had negligible effect, in agreement with other MD simulations of hydrated proteins (Steinbach and Brooks, 1993).

RESULTS AND DISCUSSION

Distributions of dihedral angles

The time evolution of the dihedral angles (ϕ, ψ) were found to be strongly dependent on hydration. The Ramachandran plots obtained for alanine at different stages of simulations, namely $t < 0.1$ ns, $0.1 \leq t < 0.2$ ns, and $0.2 \leq t < 0.3$ ns, are displayed in Fig. 1. The plots *a–c* refer to the successive results obtained with explicit hydration, and parts a'–c' to those in vacuum. The counterparts of these plots for glycine are shown in Fig. 2. (ϕ, ψ) angle pairs of all residues in pAla except the terminal ones are included in Fig. 1, whereas only the middle five glycines of pGly are considered in obtaining Fig. 2. Serine and valine were found to yield dihedral angle distributions similar to Ala, and therefore are not shown.

First, let us examine the results obtained with explicit hydration. The results for pAla-*w* and pGly-*w* in the interval

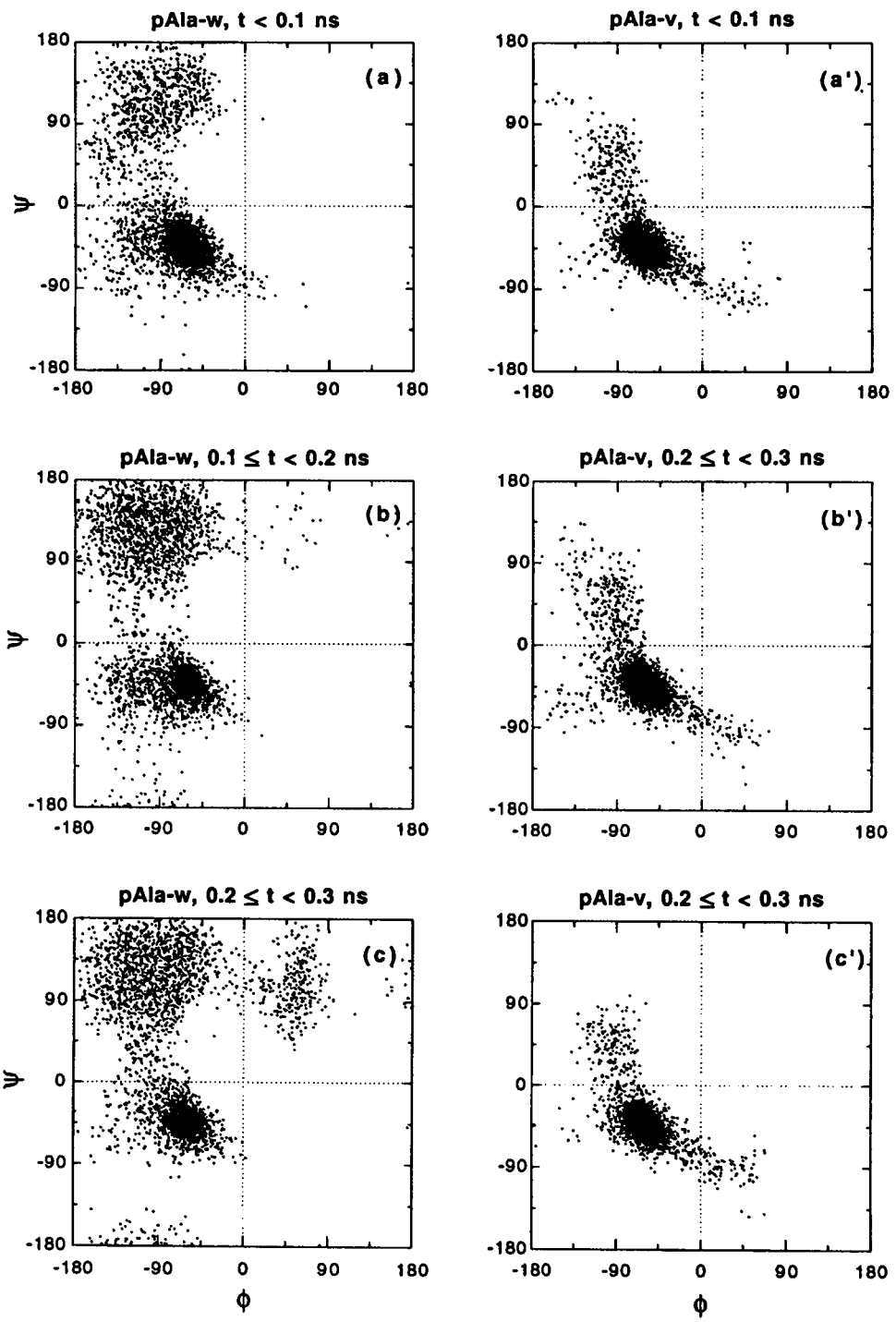

FIGURE 1 Distribution of backbone dihedral angles of Ala residues observed at various stages of MD simulations of pAla. The backbone dihedral angles are set to their α-helical values before equilibration and the MD simulations. The plots *a*, *b*, and *c* are obtained for the simulations in water at the respective time intervals of $t < 0.1$ ns, $0.1 \leq t < 0.2$ ns $0.2 \leq t < 0.3$ ns. The counterparts of these plots obtained in vacuo are shown in a', b', and c'. The plots *c* and c' represent the equilibrium distributions with explicit hydration and in vacuo, respectively.

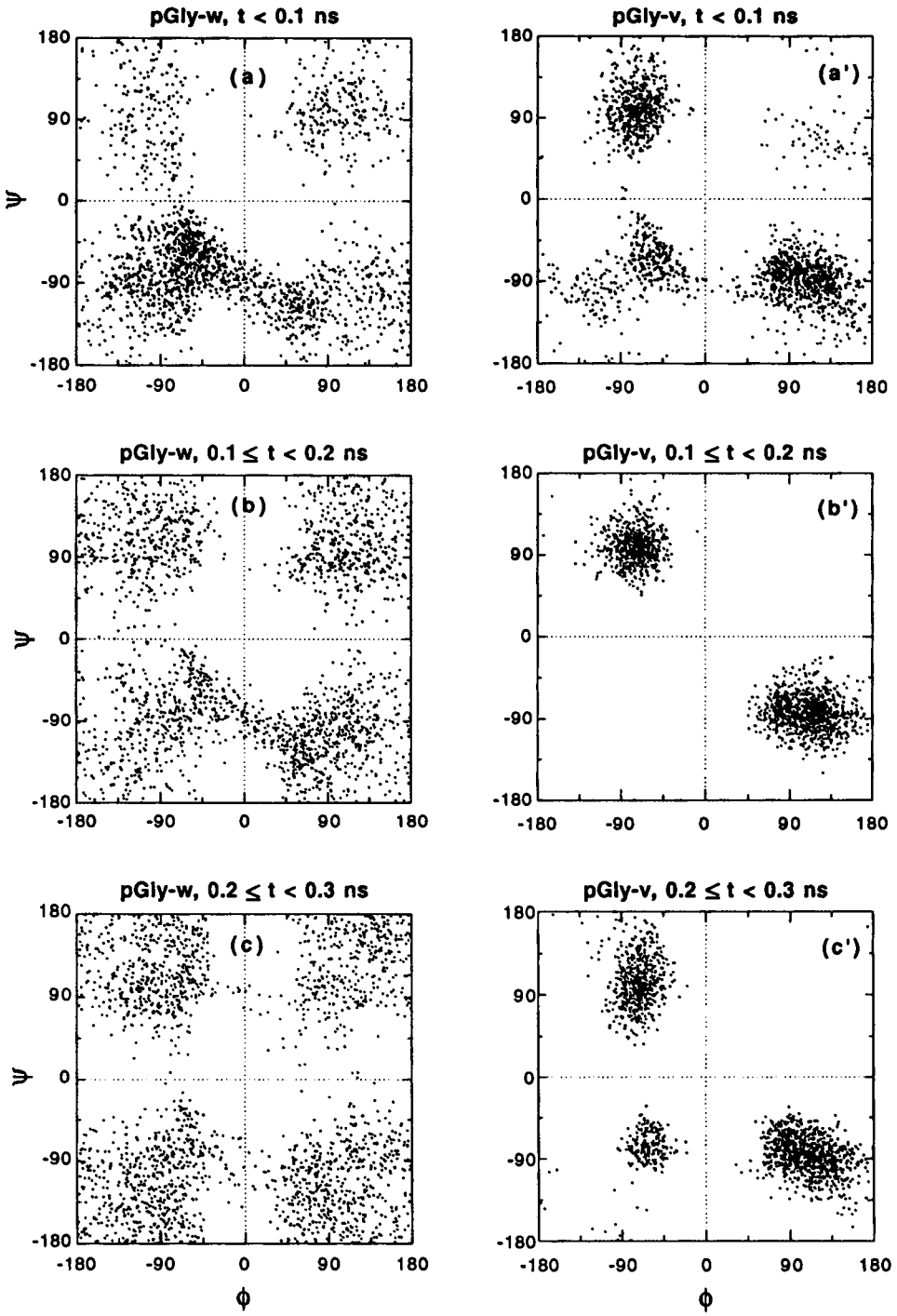

FIGURE 2 Time evolution of the distribution of the backbone dihedral angles of Gly residues observed in the MD simulations of pGly. The backbone dihedral angles are set to their α-helical values before equilibration and MD simulations. See legend to Fig. 1 for the description of the plots (a, b, c, a', b', and c').

$0.2 \leq t < 0.3$ ns, shown in parts c of the two figures, exhibit the well-known characteristics of the classical Ramachandran plots, conforming with the identifications of Ala and Gly as helix-forming and breaking amino acids, respectively. The α-helical region is highly populated in parts a, because of the choice of all helical initial conformers. In Ala, the β-sheet region is gradually populated as the simulation proceeds, as may be observed from Fig. 1 b; this phase is succeeded by the sampling of the left-handed α-helical region of the conformational space in part c. In the case of glycine (Fig. 2), the upper left, lower right, and upper right quadrants of the dihedral angle plots are successively populated, as may be verified from parts a–c. The bias from the original helical structures apparently disappears after a MD run of 0.2 ns in water.

The final distributions (c') attained in vacuum simulations exhibit a striking departure from their counterparts c obtained with explicit hydration. For example, a predominance of the α-helical state is distinguished for pAla-v, which suggests that the original secondary structure is sub-

stantially more persistent in the absence of water molecules. pGly-*v*, on the other hand, exhibits an excessive tendency to populate the upper left and lower right quadrants. The asymmetry of the (ϕ, ψ) plot for pGly-*v* ($0.2 \leq t < 0.3$ ns) persisted throughout a longer duration (1 ns) run. Thus, glycine residues cannot effectively sample the configurational space in vacuo, but remain trapped in local energy minima.

We note that the pair of dihedral angles (ϕ, ψ) $\approx$ ($-90°$, 90°) for the *i*th residue is characteristic of the C_7^{eq} structure, a seven-atom ring completed by a hydrogen bond between $(CO)_{i-1}$ and $(NH)_{i+1}$ (Mezei et al., 1985). This pair of dihedral angles and its symmetric counterpart (90°, $-90°$), are strongly favored in pGly-*v*, as illustrated in Fig. 2, parts *a'*–*c'*. This is consistent with the strong tendency of the polypeptide to satisfy all hydrogen bond-forming groups. Such a strong bias for intramolecular hydrogen bond formation was not observed in the runs with explicit hydration, *a*–*c*, the polypeptide polar groups being in this case satisfactorily solvated by water molecules. Neglect of explicit hydration thus favors intramolecular hydrogen bonds. A result is the tendency of the molecule to assume relatively more compact conformations, a commonly observed bias in vacuum simulations of proteins or polypeptides.

Solvent effects on the time evolution of helical fragments

The distance between the *i*th carbonyl group and the (*i*+4)th amide group is used as a criterion for helical state with a value of 2.3 Å adopted as an upper limit for the separation between the two groups. Occurrences of seven possible (i, i + 4) hydrogen bonds in pAla, pVal, and pSer are inspected at each snapshot of 300-ps independent MD runs. The fractions of unperturbed (i, i + 4) pairs are determined as a function of time.

Figs. 3*a*–*c* display the percentage of helical residues, or more precisely $(CO)_i$ and $(NH)_{i+4}$ pairs forming hydrogen bonds characteristic of α-helices, plotted at 3.0-ps intervals. Results are shown for Ala, Val, and Ser in parts *a*–*c*, respectively. The lightface and boldface curves refer to the respective behaviors in vacuo and with explicit hydration. The curve for glycine exhibits a precipitous drop to zero within picoseconds, and therefore it is not shown.

A significant fraction of helical residues unfolds during the equilibration, such that the percentage of helical residues starts from $\leq$70% at $t = 0$. After this initial drop, the curves for Ala and Val are found to approximate an exponential time decay. The characteristic times for the unwinding of pAla-*w* and pVal-*w* are found to be 396 and 307 ps, respectively, with correlation coefficients of 0.905 $\pm$ 0.05, from the fitting of the corresponding decay curves in Fig. 3 by single exponentials in the range $0 < t < 300$ ps. pSer-*w*, on the other hand, levels off to an asymptotic value within the first 50 ps.

The rank order Ala > Val > Ser > Gly is manifested in the unfolding rates of polypeptides. Ala and Val exhibit

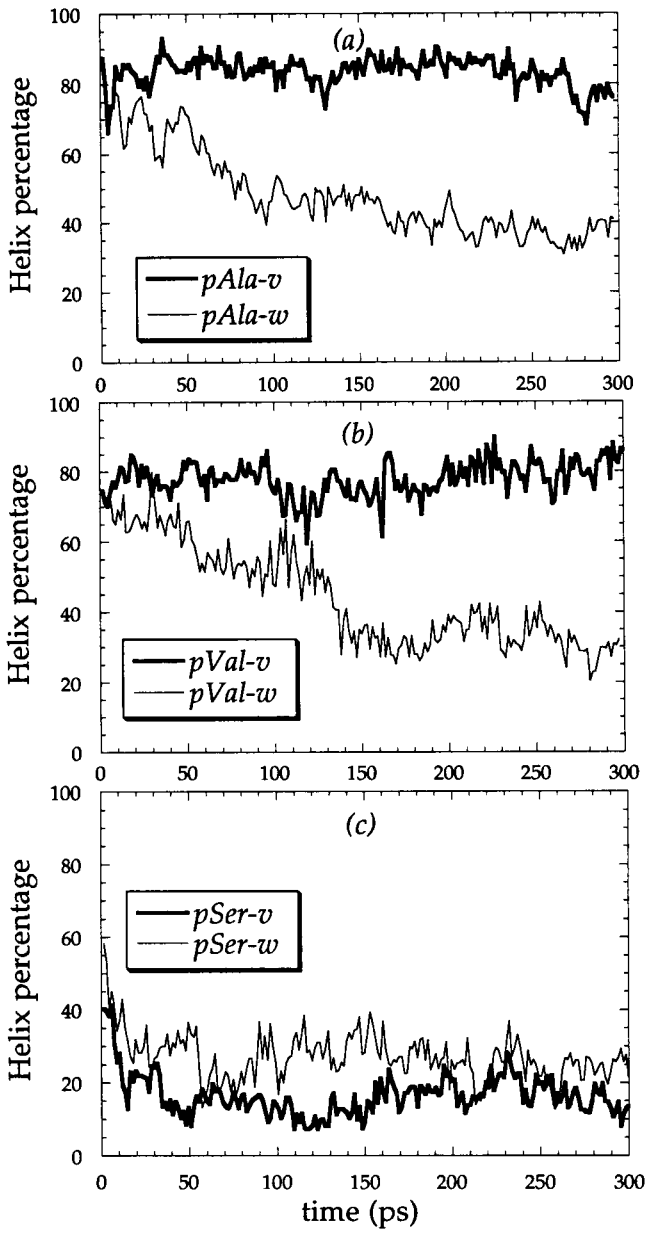

FIGURE 3 Time evolution of the fraction of residues having α-helical structure observed for (*a*) Ala, (*b*) Val, and (*c*) Ser, from the MD simulations of pAla, pVal, and pSer in vacuum (*boldface curve*) and with explicit hydration (*lightface curve*). Hydration is observed to have opposite effects on the stability of Ser helices compared to Ala and Gly, as can be seen from the two time decay curves obtained for the two environments.

similar kinetics, both in vacuum and in water, indicating that the energy barriers to be surmounted by these residues during helix unwinding are comparable in magnitude.

The adoption of a collapsed (or unified) atom approximation for methyl groups in the standard parameter set 37C4 of GROMOS87 presently used may have diminished the steric effects that destabilize the original helical state of valine, resulting in a slowing down of the unwinding of pVal. Previous comparison of helix stabilities of alanine and valine (Yun and Hermans, 1991) indicated that the free

energy difference between the coil and helix states of Val exceeds that of Ala by $\Delta\Delta G$ = 3.4 kJ/mol if full atomic interactions are taken into consideration for the methyl groups; whereas $\Delta\Delta G$ reduces to 0.6 kJ/mol if a central atom potential conforming with the collapse of hydrogens onto the methyl carbon atom is adopted. It is likely that a decrease in the free energy of the initial (helical) state of valine due to the unified atom model has induced here an increase in activation energy, and thus moderated the unwinding rate of pVal helices. Simulations of pVal repeated by increasing the van der Waals radii of the CH_3 groups indicate, in fact, an enhancement in helix unwinding. A reduction in the intrinsic torsional barrier of C^{α}—C^{β} bond was also found to accelerate the unwinding. These tests demonstrate that the steric effects associated with the side chain, and the enhanced rotational mobility of the side groups, may contribute to the destabilization of valine helices. Nevertheless, we chose to do simulations with the 37C4 force field of GROMOS87. The van der Waals parameters for CH_3 therein closely match those of the newer version of the same package (force field 43A1 of GROMOS96), and the C^{α}—C^{β} bond torsion potential parameters are left unchanged (van Gunsteren et al., 1996).

The unfolding rates of pAla and pVal helices are significantly enhanced when explicit water molecules are introduced. The model polypeptide pSer, on the other hand, exhibits the opposite behavior with regard to the effects of water: pSer helix is rapidly unwound in vacuo, while the unwinding is observed to be slower in the presence of water molecules. Therefore, the fast unwinding of Ser is intrinsic to the residue itself. This property is related to the tendency of the —OH side groups to form hydrogen bonds with the carbonyl groups, thus breaking the hydrogen bonds stabilizing the α-helices. In the presence of water, some of the OH groups are caught in hydrogen bonds with water, and consequently the competition of such backbone-side group hydrogen bonds for backbone hydrogen bonds is weaker, which explains the relative positions of the two curves in Fig. 3 *c*.

The number of hydroxyl groups forming a hydrogen bond with backbone carboxyl groups in pSer were counted as 4290 in vacuo and 372 in water, using the results from two independent runs for each environment. This indicates immediately the stronger tendency to form intramolecular hydrogen bonds in vacuo at the expense of those stabilizing the α-helical states. Fifty-nine percent of the intramolecular hydrogen bonds occur between OH and CO groups, while the remaining 41% are backbone-backbone hydrogen bonds. Among the hydrogen bonds formed between OH and CO groups, 41.6% occur between the OH of residue i and the CO of residue (i−4), and 24.1% between the respective groups of residues i and i−3. This is further evidence that the hydroxyl side group of Ser competes effectively with the backbone amide group in helices and eventually displaces the amide to form a hydrogen bond with the carbonyl group.

Distribution of water molecules around alanine, valine, serine, and glycine

The radial distribution functions $g(r)$ for water oxygen atoms in the neighborhood of side group atoms of different types are displayed in Fig. 4. The distributions are calculated for the C^{β} atoms of Val and Ala, O^{γ} atoms of Ser, and C^{γ} atoms of Val. The subset of residues whose dihedral angles lie in the ranges $-100° \leq \phi \leq -25°$ and $-80° \leq \psi \leq -5°$ are considered (Daggett and Levitt, 1992) here, in order to visualize the clustering of water molecules around helical fragments. The ordinate represents the number of water oxygens located within spherical shells of radius r and thickness 0.2 Å centered about the atoms of interest, averaged over various snapshots and normalized upon division by r^2 first, and then with respect to the asymptotic value at $r \approx 10$ Å.

The distributions of water molecules near helices exhibit residue-specific characteristics: the β-carbon of Val is quite protected from water, the most probable separation being ~4 Å. This is due to the steric hindering of the C^{γ} atoms, whereas water molecules come closer (~3.5 Å) to the β-carbon of Ala. The fact that the C^{β} atom of Val is less accessible to water compared to the same atom in Ala implies that the pAla backbone is more open to hydration effects, which might destabilize the helical hydrogen bonds, compared to pVal. The hydroxyl oxygen of Ser, on the other hand, is highly susceptible to hydrogen bond formation with water, as the peak at ~2.7 Å reveals. In the figure inset, the distribution for the C^{γ} atom of Val is shown to be superimposable upon that of Ala C^{β}, demonstrating that the solvation of the terminal methyl groups are almost identical, regardless of the residue type.

In crystal structures, the peaks for the first hydration shell around the C^{β} atoms of Ala and the C^{γ} atom of Val are

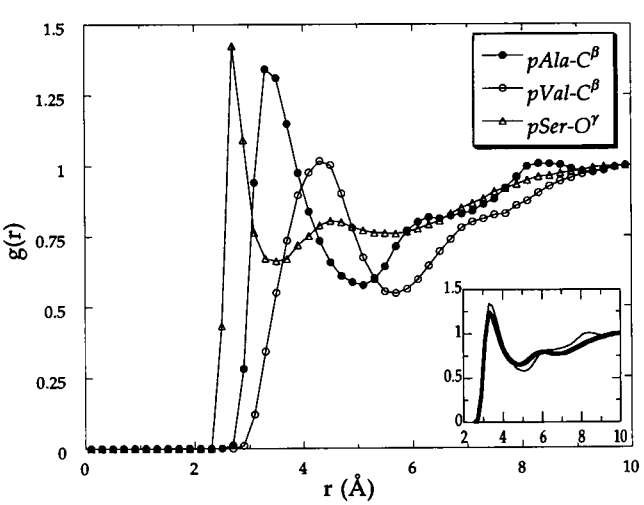

FIGURE 4 Radial distribution functions $g(r)$ for water molecules around the C^{β} atoms of Ala and Val, and the O^{γ} atom of Ser, as indicated in the label, the backbone being α-helical in all cases. The inset compares the distributions obtained for the C^{β} atom of Ala (*lightface*) and the C^{γ} atom of Val (*boldface*).

found to be in the range 3.8–4.0 Å (Walshaw and Goodfellow, 1993), and the first hydration shell around the β-carbon of Val is shifted to 4.3–4.5 Å. Present MD runs yield values lower by ~0.5 Å, presumably due to the adoption of unified atom approximation. This conforms with previous remarks (Smith et al., 1995) on modifying the Lennard-Jones repulsive energy parameters between carbon atoms and SPC water oxygens in order to better mimic the hydration of carbon atoms.

We also examined the angular distribution for water molecules, $g(\vartheta)$, in the range $r < 5$ Å, around different side groups. $g(\vartheta)$ around the O^{γ} atom of serine (not shown) exhibits a peak at 75°, approximating a tetrahedral packing. Here, ϑ denotes the supplement of the angle between C^{β}—O^{γ} and $O^{\gamma}\cdots$O(water). The distributions from crystal structures (Thanki et al., 1988) show a similar peak at 65° and a broad excluded region >120°, which is due to the steric overlap with the backbone. Likewise, $g(\vartheta)$ around C^{β} of alanine (not shown) exhibits a peaks at 85° and an excluded region in the range $140° < \vartheta < 180°$, in good agreement with results from crystal structures (Walshaw and Goodfellow, 1993). For alanine, ϑ refers to the angle between C^{α}—C^{β} and $C^{\beta}\cdots$O(water).

The complete description of the position of the water molecules relative to the backbone also necessitates the specification of the azimuthal angle φ. Following the definition of Walshaw and Goodfellow, φ is the angle that the projection of r on a plane perpendicular to the bond C^{α}—C^{β} makes with the plane defined by the consecutive bonds C^{α}—C^{β} and C^{α}—N. Present MD runs yielded bimodal distributions with peaks around ±90°, with a larger number of water molecules at negative φ values, and some volume exclusion at $\varphi = 0°$ and ± 180°, which is due to the interference with the polar groups of the neighboring residues along the backbone. These results are similar to those extracted from crystal structure data (Walshaw and Goodfellow, 1993).

Correlation between destabilization of helices and formation of hydrogen bonds between polar backbone groups and water

The solvation of the polar groups of the polypeptide backbone are analyzed here in terms of the two-dimensional pair distribution functions $g(r, \theta)$ of water molecules around carbonyl oxygens. The distributions $g(r, \theta)$ are determined for two distinct sets of conformers for a given residue, shortly referred to as helix and coil, identified on the basis of the (i, i + 4) intramolecular hydrogen bond, as previously described. $g(r, \theta)$ thus reflect the hydration of the particular amino acid before and after the disruption of helical structure. Here r is the distance between the carbonyl O and the water H (the one closer to carbonyl oxygen among the two H of H_2O), shortly referred to as O· · ·H distance. θ is the supplement of the angle between C═O and O· · ·H. Grids of size $\Delta r = 0.2$ Å and $\Delta\theta = 3.6°$ in the ranges $r \leq 10$ Å and $0 \leq \theta \leq 180°$ are examined at 0.25-ps intervals for evaluating the average numbers of O· · ·H pairs. These numbers are divided by $r^2\sin\theta$, so as to remove the biases arising from the different volumes of the successive shells and from the uniform distribution (½)sin θ over θ. The results are referred to as the *normalized* distributions $g(r, \theta)$.

Figs. 5 *a* and *b* compare the hydration patterns around the carbonyl oxygen of Val before and after disruption of the (i, i + 4) hydrogen bonds. Both the three-dimensional plots and the corresponding contours are shown for clarity. The most striking difference between the surfaces *a* and *b* is the appearance of a broad peak in the vicinity of $r = 2$ Å, $0 \leq \theta \leq 50°$ in the coil state, which is altogether absent in the helix state. This particular geometry, i.e., ~2 Å separation between C═O oxygen and water H, and ~25° angular deflection between C═O and O· · ·H, is typical of hydrogen

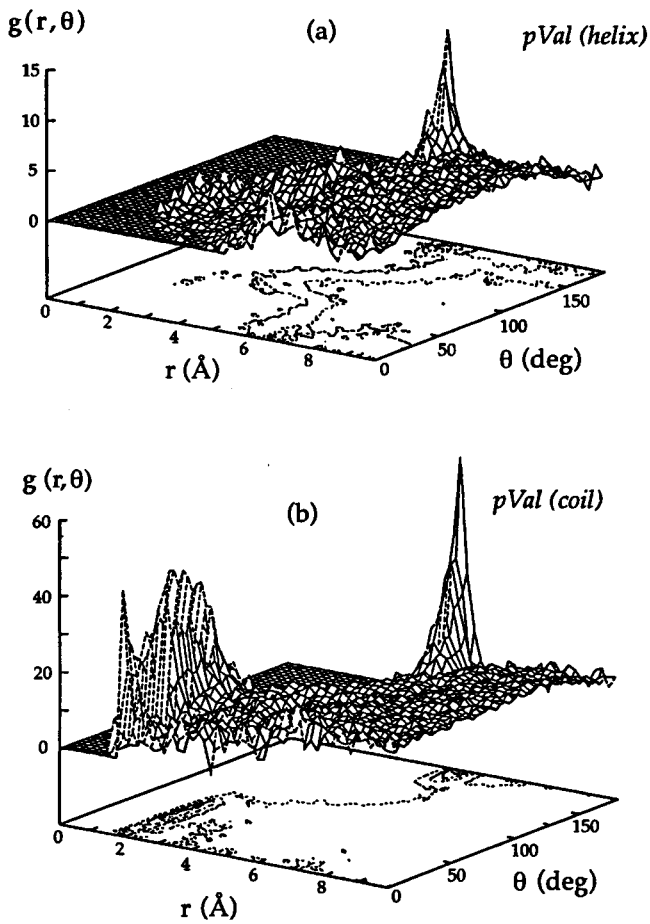

FIGURE 5 Two-dimensional distribution functions $g(r, \theta)$ for the hydration patterns around the carbonyl oxygen of Val before (*a*) and after (*b*) disruption of the α-helical state. The horizontal axes represent the geometric variables r and θ. r is the distance between carbonyl O and nearest water H atoms, referred to as the O· · ·H distance; θ is the supplement of the angle between C═O and O· · ·H. The vertical axes represent the number distribution of water molecules (or O· · ·H pairs) normalized by dividing by $r^2\sin\theta$. The contour plots are also shown for clarity. The peak in the neighborhood of $r = 2$ Å, $0 \leq \theta \leq 50°$ in the coil (*b*) state, which is altogether absent in the α-helix (*a*) state, reveals the occurrence O· · ·H water hydrogen bonds stabilizing the coil state.

bond formation. The peak appearing in part *b* is therefore direct evidence of the hydrogen bond between the backbone polar groups and the water molecules, which is implicated in the helix disruption.

Examination of the equivalent distributions for Ala and Ser indicate the same main feature, and consequently are not shown: namely, there is a direct correlation between the loci of nearest water molecules and the conformational state of the backbone; the location $r \approx 2$ Å, $0 \leq \theta \leq 50°$ emerges as a highly probable position for water molecules in all three cases (pAla-*w*, pVal-*w*, and pSer-*w*) upon destabilization of the helix structure, while the same region is barely occupied in stable helices. In the case of glycine, no comparison of two distribution surfaces is possible since the backbone does not assume the helical state to any significant extent throughout the MD runs. The only surface obtainable, that of water molecules in the neighborhood of backbone polar groups in the disordered state, is given in Fig. 6. There is no discernible peak near 2 Å, although the region $2 \leq r \leq 6$ Å is frequently visited.

Two features deserve attention in the above three-dimensional plots. 1) The vertical scale in part *a* of Fig. 5 is significantly lower than that of part *b*. This is a direct consequence of the fewer incidences of helical states for Val than coil states. The absolute height of the surface thus provides a measure of the relative probabilities of helix and coil states for the particular residues. 2) The normalization with respect to θ enhances the probability of the angles close to 0° and 180°. This effect may be eliminated by omitting the normalization with respect to θ in evaluating $g(r, \theta)$. The resulting distributions are illustrated for pAla in Figs. 7 *a* and *b*. The preference for the polar angle $\theta \approx 180°$ vanishes, in this case. However, the peak around $r = 2$ Å and $\theta = 40°$, which indicates the formation of intermolecular hydrogen bonds, persists regardless of the normalization procedure.

A closer look at the region $r \leq 3.5$ Å reveals the strong bias toward lower θ values imparted upon transition from helix to coil state, as illustrated in Fig. 8. Here, the curves are normalized so that the areas enclosed are unity in each case. The differences between the curves for different residues in a given structure are notably small. The angular distributions are thus dominated by the conformational state of the polypeptide backbone.

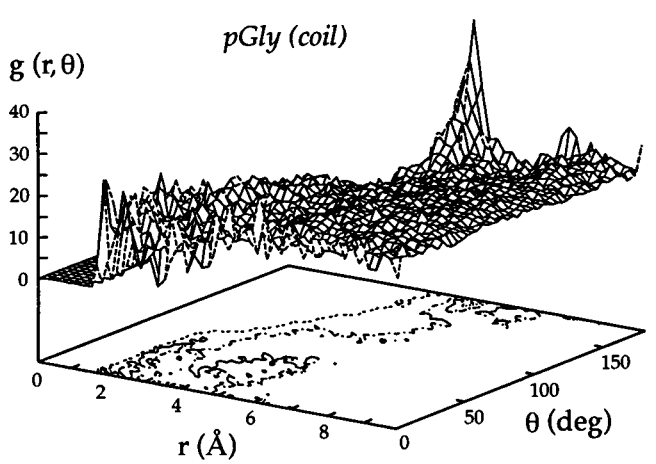

FIGURE 6 Normalized distribution $g(r, \theta)$ of water molecules around the carbonyl oxygen of Gly. See legend to Fig. 5.

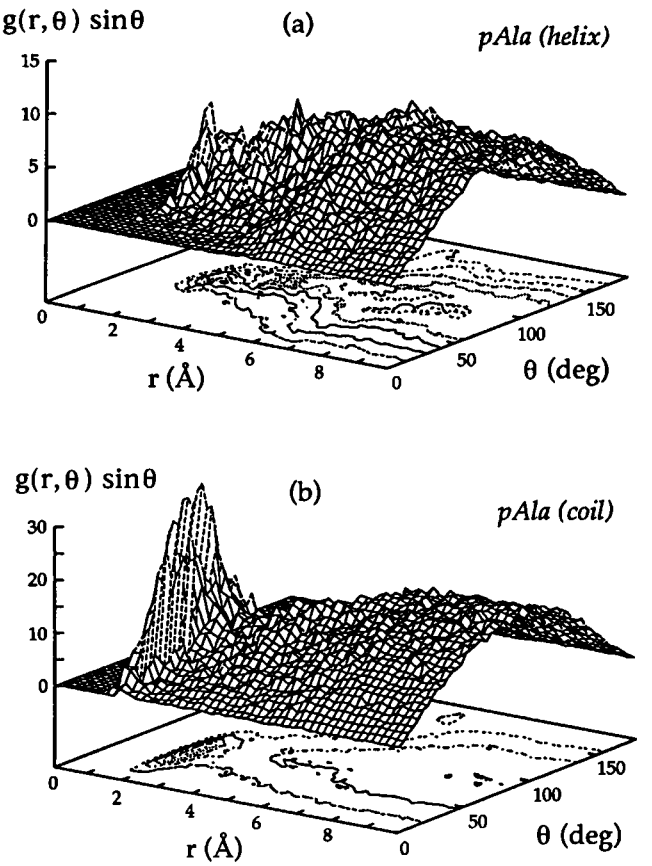

FIGURE 7 Distribution of waters around the carbonyl oxygen of Ala before (*a*) and after (*b*) disruption of the α-helical state. See legend to Fig. 5. The division by sin θ is omitted here, hence the notation $g(r, \theta)\sin\theta$ for the vertical axis. The actual θ-dependence is shown here, rather than the deviation from the homogeneous distribution that was depicted in Figs. 5 and 6. The preference for $\theta \approx 180°$ vanishes, in this case, whereas the peak around $r \approx 2$ Å, $\theta \approx 40°$, indicating the occurrence of intermolecular hydrogen bonds, persists.

Remarks on the mechanism of helix unwinding

In a survey of protein crystal structures that contain hydrated α-helices, occasional insertion of water molecules into the backbone hydrogen bond was revealed (Sundaralingam and Sekharudu, 1989) by the formation of a three-centered hydrogen bond. These structures, in which water acts as a bridge between the carbonyl and amide groups of an intact backbone hydrogen bond, were suggested to be intermediates in the folding/unfolding pathway. Later, MD simulations of polyalanine peptides (DiCapua et al., 1991) also indicated the destabilization of helices by this specific water insertion process, whereas no such process was ob-

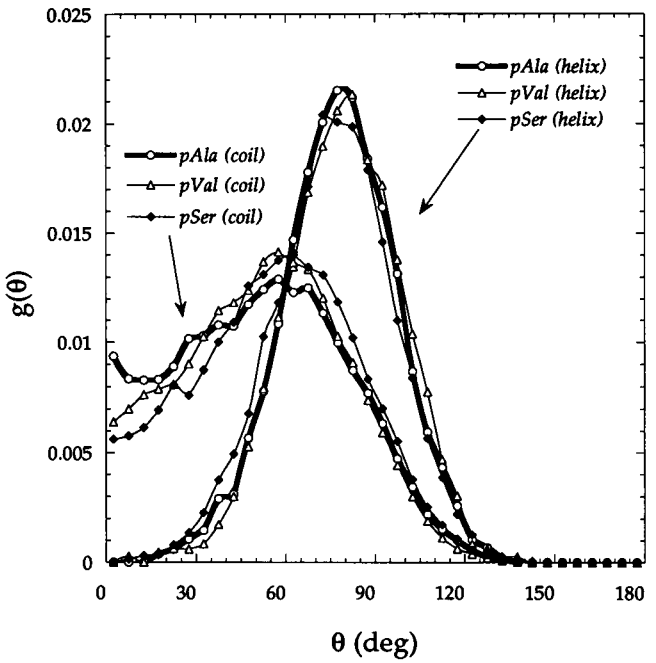

FIGURE 8 Distribution function $g(\theta)$ of the supplement of the angle between C═O bond vector and the O· · ·H separation vector for Ala, Val, and Ser in α-helix and coil states. Here, water molecules located solely in the region $r \leq 3.5$ Å are considered. The distributions are normalized such that the enclosed area is unity in each case. A strong bias toward lower θ values in favor of intermolecular hydrogen bonding geometry is imparted on passing from the helix to the coil state.

served in the case of polyglycine. In contrast, simulations of a polyalanine of 13 residues (Daggett and Levitt, 1992) have not shown any evidence of helix destabilization upon water insertion, even though a significant population of water bridges among disrupted hydrogen bonds was observed. These conform with the previous MD results of Tobias and Brooks (1991) obtained with the umbrella sampling technique. Our simulation results also support this second group. No significant occurrence of three-centered hydrogen bonds, i.e., inserted water molecules, could be observed in the present study at the exact transition point during the helix-to-coil pathway. Figs. 5*b* and 6*b* reflect, in fact, the stabilization of the coil state by hydration after the unwinding of helices, rather than the interference of water molecules at the transition state. In particular, the backbone polar groups of pVal were found to be the most protected from water molecules among the three residues Ala, Val, and Ser, both in the helix and the coil states, which implies that insertion of water molecules is altogether inapplicable in the unwinding of helical valines.

Another mechanism involved in the unwinding of α-helices was pointed out to be the replacement of (i, i + 4) hydrogen bonds typical of α-helices by (i, i + 3) hydrogen bonds between the groups $(NH)_i$ and $(CO)_{i+3}$, in conformity with the 3^{10} helical state. In order to explore the validity of this mechanism, a systematic analysis of the time evolution of the distances $r(O_i–H_{i+4})$ and $r(O_i–H_{i+3})$ has been carried out for all residues originally participating in α-helices. A distance range of $r \leq 2.3$ Å between these atoms is again accepted as a criterion of hydrogen bond formation. Our analysis reveals that in pAla in particular, the replacement of (i, i + 4) hydrogen bonds by (i, i + 3) hydrogen bonds is a rather frequent feature at the onset of the unwinding of α-helices. Almost half of the disruptions of (i, i + 4) hydrogen bonds in pAla and pVal in water are found to be accompanied by (i, i+3) hydrogen bond formation. Fig. 9 *a* displays, for example, a portion of a trajectory for a bond *i*

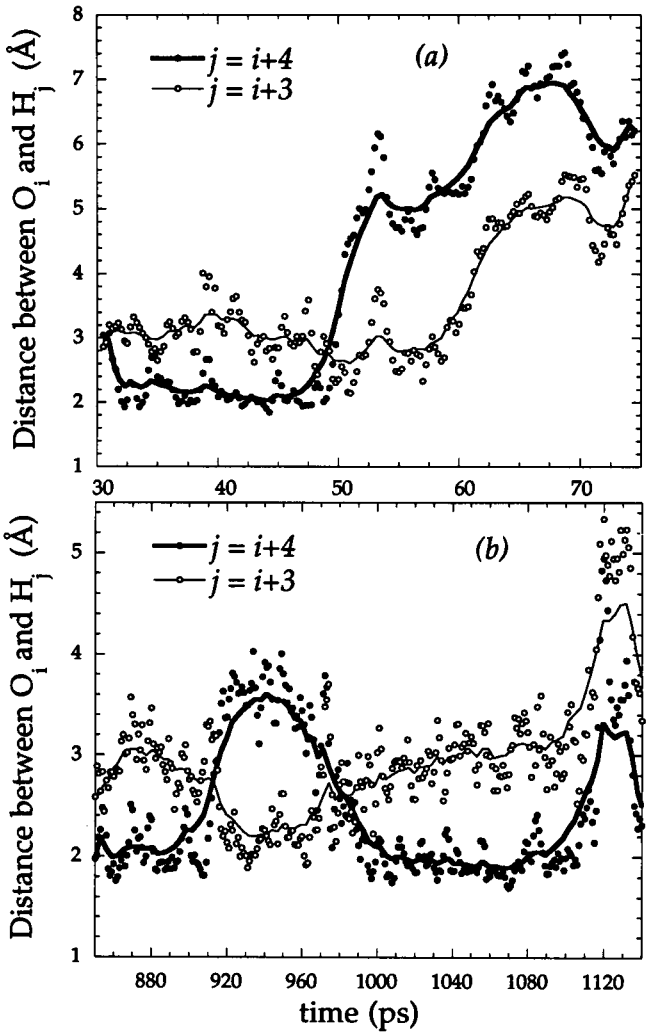

FIGURE 9 Portions of MD trajectories from (*a*) pAla-*w* and (*b*) pVal-*w* illustrating the transition from α-helix to coil state for a given amino acid i. Unwinding of the α-helical state, as probed by the disruption of the (i, i + 4), is accompanied in both cases by the formation of (i, i + 3) hydrogen bonds. Filled and open circles refer to the distances $r(O_i–H_{i+4})$ and $r(O_i–H_{i+3})$ data recorded at 0.25-ps intervals. In part *a*, an abrupt increase in $r(O_i–H_{i+4})$ from 2 to 6 Å, approximately, is observed at the transition. We note the decrease in the distance $r(O_i–H_{i+3})$ to ~2.0 Å at the onset of the α-helix unfolding, followed by the stabilization of the intermediate 3^{10} helix form by (i, i+3) hydrogen bonds. The complete unwinding is indicated by an increase in both $r(O_i–H_{i+4})$ and $r(O_i–H_{i+3})$. Part *b* illustrates the successive cross-overs between the two helical forms, suggesting that the 3^{10} helix state may also be an intermediate in the folding pathway of α-helices.

belonging to pAla-*w*, illustrating a transition from α-helix to coil state accompanied by the formation of (i, i + 3) hydrogen bonds at the onset of the transition. The filled circles and open circles represent the instantaneous $r(O_i–H_{i+4})$ and $r(O_i–H_{i+3})$ distances, respectively, recorded at 0.25 ps intervals. Smooth curves are drawn through the data to guide the eye. Originally, $r(O_i–H_{i+4})$ is ~2.0 Å, as required for (i, i + 4) groups participating in α-helix. The transition to coil state starts at ~48 ps, and is completed within 10 ps, approximately. It is interesting to notice that the distances $r(O_i–H_{i+4})$ and $r(O_i–H_{i+3})$ become equal to each other at the onset of transition, which was a common feature examined in all disruption of α-helical amino acids via (i, i + 3) hydrogen bond formation. This is succeeded by a close association of the (i, i + 3) groups, conforming with the intermediate state stabilized with (i, i + 3) hydrogen bonds. In addition to such helix-to-coil transitions, interconversions between (i, i + 4) and (i, i + 3) hydrogen bonds were also observable, in some cases, suggesting that the formation of (i, i + 3) hydrogen bonds is equally operative in the folding pathway of α-helices. Part *b* of Fig. 9 illustrates one such example of interconversions between (i, i + 4) and (i, i + 3) hydrogen bonds observed in a run of pVal in water.

A careful examination of Fig. 9 shows that fluctuations of considerable amplitude occur in the atomic positions, and particularly in the separation between hydrogen bond-forming polar groups characteristic of α-helices, before the disruption of α-helices. The same feature was also observed for the fluctuations of dihedral angles (Fig. 3), demonstrating that relatively high amplitude torsional oscillations, and even occasional rotational jumps, take place inducing rapid interconversions between helix and coil states before the final stabilization of the coiled state. Our analysis shows that among this multitude of transitions, only those stabilized by solvation (i.e., hydrogen bond formation with water molecules) or by favorable intramolecular interactions [e.g., hydrogen bond formation between (i, i + 3) backbone polar groups, or between $(OH)_i$ and $(CO)_{i-4}$ for serine] are persistent and lead to the complete unwinding of the helix.

We note that free energy calculations (Tobias and Brooks, 1991), and MD simulations at various temperatures (Daggett and Levitt, 1992), indicated a barrier height of ~2.0 kcal/mol for the helix-to-coil transition of alanine. Insofar as the free energy level of the activated state between helix and coil states is concerned, Tobias and Brooks pointed out that valine-rich helices destabilize faster over alanine-based analogs due to a favorable solvation component in the intermediate (reverse turn) state. Accordingly, the transition from helix to coil (or extended) state is done by a passage through an intermediate metastable state, the reverse turn, the free energy barriers for the successive steps helix-to-turn and turn-to-extended being 1.1 and 2.1 kcal/mol, respectively. The same reaction coordinate is found to involve the respective free energy barriers of 1.9 and 1.2 kcal/mol in the case of alanine (Tobias and Brooks, 1991). These results suggest that the complete unfolding of valine residues occurs within a time scale comparable to that of alanine, in spite of the faster initiation of the unwinding of valine. In the present simulations, the initiation of unfolding is of the order of picoseconds in both pVal and pAla, as the original drop in the curves indicates. The global unwinding, on the other hand, occurs in the range of hundreds of picoseconds, as shown above, both for pAla and pVal, confirming the occurrence of an effective activation energy of comparable magnitude.

CONCLUSIONS

The major conclusions of the present study are summarized as follows. First, the effect of the aqueous environment on the unfolding of α-helices is highly residue-specific. The unwinding of Ala and Val α-helices is accelerated in water compared to in vacuo. Ser, on the other hand, exhibits the opposite behavior. Its helix conformation is rapidly disrupted in vacuo, while a net decrease in the unwinding rate is observed with explicit hydration. In fact, water molecules compete with intramolecular hydrogen bonds and eventually break them, in the case of Ala and Val in helices; but in Ser, the intramolecular hydrogen bonds of helices are already substantially destabilized by the side-group hydroxyl groups, which exhibit a strong tendency to form side-group-backbone hydrogen bonds with the C═O group of the third or fourth preceding residue. Water molecules attenuate this effect by capturing some hydroxyl groups.

Second, both the time evolution and the equilibrium distribution of dihedral angles are affected by hydration. The equilibrium distributions of dihedral angles in water approximate the conventional Ramachandran plots, whereas in vacuo Ala exhibits a strong preference for the α-helical state. Likewise, in vacuo Gly remains trapped in local energy minima stabilized by a hydrogen bond between $(CO)_{i-1}$ and $(NH)_{i+1}$.

Third, a rank of Gly > Ser > Val ≥ Ala is observed in the rate of unwinding of the helical states of the four investigated residues. The breakup of pAla and pVal helices in water is completed on the order of tenths of nanoseconds, conforming with previous predictions (Brooks and Case, 1993), whereas pSer unfolds within ~50 ps. Two counter effects operate in determining the unwinding kinetics of Val relative to Ala: the backbone is more protected from the destabilizing effect of water molecules due to the presence of γ-carbons, as the pair radial distribution functions demonstrate. On the other hand, the bulkier side chain of Val tends to disrupt the tight packing in the helical state.

Fourth, there is a direct correlation between the conformational state of the polypeptide backbone and the loci of water molecules in the close neighborhood, except for pGly. This may be verified from a comparison of the two-dimensional spatial distributions displayed in parts *a* and *b* of Figs. 5 and 7. In parts *b*, which reflect the behavior after the disruption of the helical order, the hydrogen atoms of water molecules exhibit a strong preference for the region $r = 2.0$

Å, $\theta < 40°$ with respect to the backbone polar groups, which is a geometry suitable for intermolecular hydrogen bond formation, whereas such a preference is hardly distinguishable when the backbone assumes the helical state in part *a*.

Fifth, interconversions between (i, i + 3) and (i, i + 4) hydrogen bonds constitute an important mechanism of α-helix unwinding/winding. The interatomic distances, or the rotational angles ϕ and ψ of the backbone bonds, are observed to be subject to fluctuations of substantial amplitude throughout simulations. These vibrational motions around the equilibrium state lead to occasional disruptions of the hydrogen bonds (i, i + 4) stabilizing α-helices, which may or may not be restored depending on the simultaneous occurrence of hydrogen bonds stabilizing other structures. Examples for the latter are the hydration of backbone polar groups leading to more extended conformations, the formation of hydrogen bonds between backbone polar groups i and (i + 3) characteristic of 3^{10} helices, or between backbone $(CO)_{i-4}$ and side-chain $(OH)_i$ groups as in the case of serine, or $(CO)_{i-1}$ and $(NH)_{i+1}$ around glycine.

The authors are indebted to Drs. R. L. Jernigan and B. Erman for critical reading of the manuscript and offering many helpful suggestions.

Partial support by Bogazici University Research Funds Project #96P003 and by the Turkish Academy of Sciences is gratefully acknowledged.

REFERENCES

Andersen, A., and J. Hermans. 1988. Microfolding: conformational probability map for the alanine dipeptide in water from molecular dynamics simulations. *Proteins*. 3:262–265.

Bahar, I., P. Doruker, and B. Badur. 1993. Solvent effect on translational diffusivity and segmental orientational mobility of polymers in dilute solution: a molecular dynamics study. *J. Chem. Phys.* 99:2235–2246.

Berendsen, H. J. C., J. P. M. Postma, W. F. van Gunsteren, and J. Hermans. 1981. Interaction models for water in relation to protein hydration. *In* Intermolecular Forces. B. Pullman, editor. Reidel, Dordrecht. 331–342.

Berendsen, H. J. C., J. P. M. Postma, W. F. van Gunsteren, A. Di Nola, and J. R. Haak. 1984. Molecular dynamics with coupling to an external bath. *J. Chem. Phys.* 81:3684–3690.

Bierzynski, A., P. S. Kim, and R. L. Baldwin. 1982. A salt bridge stabilizes the helix formed by isolated C-peptide of RNase A. *Proc. Natl. Acad. Sci. USA*. 79:2470–2474.

Blaber, M., X. Zhang, and B. W. Matthews. 1993. Structural basis of amino acid α-helix propensity. *Science*. 260:1637–1640.

Bradley, E. K., J. F. Thomason, F. E. Cohen, P. A. Kosen, and I. D. Kuntz. 1990. Studies of helical peptides using circular dichroism and nuclear magnetic resonance. *J. Mol. Biol.* 215:607–622.

Brant, D. A., W. G. Miller, and P. J. Flory. 1967. Conformational energy estimates for statistically coiling polypeptide chains. *J. Mol. Biol.* 23: 47–65.

Brooks III, C. L., and D. A. Case. 1993. Simulations of peptide conformational dynamics and thermodynamics. *Chem. Rev.* 93:2487–2502.

Brown, J. E., and W. A. Klee. 1971. Helix-coil transition of the isolated amino terminus of ribonuclease. *Biochemistry*. 10:470–476.

Chakrabartty, A., and R. L. Baldwin. 1995. Stability of α-helices. *Adv. Protein. Chem.* 46:141–176.

Chakrabartty, A., T. Kortemme, and R. L. Baldwin. 1994. Helix propensities of the amino acids measured in alanine-based peptides without helix-stabilizing sidechain interactions. *Protein Sci.* 3:843–852.

Chou, P. Y., and G. D. Fasman. 1978. Empirical predictions of protein conformation. *Annu. Rev. Biochem.* 47:251–276.

Daggett, V., P. A. Kollman, and I. D. Kuntz. 1991. A molecular dynamics simulation of polyalanine: an analysis of equilibrium motions and helix-coil transitions. *Biopolymers*. 31:1115–1134.

Daggett, V., and M. Levitt. 1992. Molecular dynamics simulations of helix denaturation. *J. Mol. Biol.* 223:1121–1138.

DiCapua, F. M., S. Swaminathan, and D. L. Beveridge. 1990. Theoretical evidence for destabilization of an α-helix by water insertion: molecular dynamics of hydrated decaalanine. *J. Am. Chem. Soc.* 112:6768–6771.

DiCapua, F. M., S. Swaminathan, and D. L. Beveridge. 1991. Theoretical evidence of water insertion in α-helix bending: molecular dynamics of Gly_{30} and Ala_{30} in vacuo and in solution. *J. Am. Chem. Soc.* 113: 6145–6155.

Doruker, P., and I. Bahar. 1993. Effect of intrachain constraints and polymer-solvent interactions on chain statistics and dynamics. *Comp. Polymer Sci.* 3:87–97.

Hermans, J., A. G. Anderson, and R. H. Yun. 1992. Differential helix propensity of small apolar side chains studied by molecular dynamics simulations. *Biochemistry*. 31:5646–5653.

Horovitz, A., J. M. Matthews, and A. R. Fersht. 1992. α-Helix stability in proteins. II. Factors that influence stability at an internal position. *J. Mol. Biol.* 227:560–568.

Huyghues-Despointes, B. M. P., J. M. Scholtz, and R. L. Baldwin. 1993. Helical peptides with three pairs of Asp-Arg and Glu-Arg residues in different orientations and spacings. *Protein Sci.* 2:80–85.

Kim, P. S., and R. L. Baldwin. 1984. A helix stop signal in the isolated S-peptide of ribonuclease A. *Nature*. 307:329–334.

Lyu, P. C., M. I. Liff, L. A. Marky, and N. R. Kallenbach. 1990. Side chain contributions to the stability of alpha-helical structure in peptides. *Science*. 250:669–673.

Lyu, P. C., L. A. Marky, and N. R. Kallenbach. 1989. The role of ion pairs in α-helix stability: two new designed helical peptides. *J. Am. Chem. Soc.* 111:2733–2734.

Marqusee, S., and R. L. Baldwin. 1987. Helix stabilization by $Glu^- \cdots Lys^+$ salt bridges in short peptides of de novo design. *Proc. Natl. Acad. Sci. USA*. 84:8898–8902.

Marqusee, S., V. H. Robbins, and R. L. Baldwin. 1989. Unusually stable helix formation in short alanine-based peptides. *Proc. Natl. Acad. Sci. USA*. 86:5286–5290.

Mezei, M., P. K. Mehrotra, and D. L. Beveridge. 1985. Monte Carlo determination of the free energy and internal energy of hydration for the alanine dipeptide at 25°C. *J. Am. Chem. Soc.* 107:2239–2245.

O'Neil, K. T., and W. F. DeGrado. 1990. A thermodynamic scale for the helix-forming tendencies of the commonly occurring amino acids. *Science*. 250:646–651.

Padmanabhan, S., S. Marqusee, T. Ridgeway, T. M. Laue, and R. L. Baldwin. 1990. Relative helix-forming tendencies of nonpolar amino acids. *Nature*. 344:268–270.

Ryckaert, J., G. Ciccotti, and H. J. C. Berendsen. 1977. Numerical integration of the Cartesian equations of motion for a system with constraints: molecular dynamics of *n*-alkanes. *J. Comp. Phys.* 23: 327–341.

Schreiber, H., and O. Steinhauser. 1992. Molecular dynamics study of solvated polypeptides: why the cutoff scheme does not work *Chem. Phys.* 168:75–89.

Smith, L. J., A. E. Mark, C. M. Dobson, and W. F. van Gunsteren. 1995. Comparison of MD simulations and NMR experiments for hen lysozyme. Analysis of local fluctuations, cooperative motions and global changes. *Biochemistry*. 34:10918–10931.

Soman, K. V., A. Karimi, and D. A. Case. 1991. Unfolding of an α-helix in water. *Biopolymers*. 31:1351–1361.

Soman, K., A. Karimi, and D. A. Case. 1993. Molecular dynamics analysis of a ribonuclease C-peptide analogue. *Biopolymers*. 33:1567–1580.

Steinbach, P. J., and B. R. Brooks. 1993. Protein hydration elucidated by molecular dynamics simulation. *Proc. Natl. Acad. Sci. USA*. 90: 9135–9139.

Sueki, M., S. Lee, S. P. Powers, J. B. Denton, Y. Konishi, and H. A. Scheraga. 1984. Helix-coil stability constants for the naturally occurring amino acids in water. 22. Histidine parameters from random poly[(hydroxybutyl)glutamine-*co*-L-histidine)]. *Macromolecules*. 17:148–155.

Sundaralingam, M., and Y. C. Sekharudu. 1989. Water-inserted α-helical segments implicate reverse turns as folding intermediates. *Science*. 244: 1333–1337.

Thanki, N., J. M. Thornton, and J. M. Goodfellow. 1988. Distribution of water around amino acid residues in proteins. *J. Mol. Biol.* 202: 637–657.

Tobias, D. J., and C. L. Brooks. 1991. Thermodynamics and mechanism of α-helix initiation in alanine and valine peptides. *Biochemistry*. 30: 6059–6070.

Tobias, D. J., S. F. Sneddon, and C. L. Brooks. 1991. The stability of protein secondary structures in aqueous solution. *In* Advanced Biomolecular Simulations. R. Lavery, J. L. Rivail, and J. Smith, editors. American Institute of Physics, New York. 174–199.

van Gunsteren, W. F., and H. J. C. Berendsen. 1987. Groningen Molecular Simulation (GROMOS) Library Manual. Biomos b.v., Nijenborgh 14, 9747 AG Groningen, The Netherlands.

van Gunsteren, W. F., S. R. Billeter, A. A. Eising, P. H. Hünenberger, P. Krüger, A. E. Mark, W. R. P. Scott, and I. G. Tironi. 1996. Biomolecular Simulation: The GROMOS96 Manual and Guide. Biomos b.v., Hochshulverlag AG an der ETH Zürich.

Walshaw, J., and J. M. Goodfellow. 1993. Distribution of solvent molecules around apolar side-chains in protein crystals. *J. Mol. Biol.* 231: 392–414.

Wang, L., T. O'Connell, A. Tropsha, and J. Hermans. 1995. Thermodynamic parameters for the helix-coil transition of oligopeptides: molecular dynamics simulation with the peptide growth method. *Proc. Natl. Acad. Sci. USA*. 92:10924–10928.

Wojcik, J., K. H. Altmann, and H. A. Scheraga. 1990. Helix-coil stability for the naturally occurring amino acids in water. *Biopolymers*. 30: 121–134.

Yun, R. H., and J. Hermans. 1991. Conformational equilibria of valine studied by dynamics simulation. *Protein Eng*. 4:761–766.

Zimm, B. H., and J. K. Brag. 1959. Theory of the phase transition between helix and random coil. *J. Chem. Phys.* 31:526–535.